



Brian E. Fischer
Integrity Applications Inc.
900 Victors Way, Suite 220
Ann Arbor, MI 48108 USA
Tel: +1 (734) 997-7436 x38
E-mail: bfischer@integrity-apps.com



Ivan J. LaHaie
Integrity Applications Inc.
900 Victors Way, Suite 220
Ann Arbor, MI 48108 USA
Tel: +1 (734) 997-7436 x724
E-mail: ilahaie@integrity-apps.com

Introduction

Of crucial importance to the development of improved inversion (and related) algorithms is the availability of quality measured data, and the information that describes it. This month's Measurements Corner paper describes a database of calibrated data meant to further the goals of scholarly research in inversion (imaging) algorithms worldwide. In particular, a database for a near-field multi-static microwave-tomography system is presented.

The University of Manitoba Microwave Imaging Repository: A Two-Dimensional Microwave Scattering Database for Testing Inversion and Calibration Algorithms

Colin Gilmore¹, Amer Zakaria², Puyan Mojabi², Majid Ostadrahimi², Stephen Pistorius^{1,3}, and Joe LoVetri²

¹Medical Physics
CancerCare Manitoba
675 McDermot Avenue
Winnipeg, Manitoba, Canada
Tel: +1 (204)787-2197; E-mail: colin.g.gilmore@gmail.com; Stephen.Pistorius@cancercare.mb.ca

²Electrical and Computer Engineering
University of Manitoba
Room E2-390 Engineering Information and Technology Complex
75 Chancellor's Circle
Winnipeg, Manitoba, Canada
Tel: +1 (204) 474-9603
E-mail: azakaria@ee.umanitoba.ca; pmojabi@ee.umanitoba.ca; morahimi@ee.umanitoba.ca; Joe_LoVetri@umanitoba.ca

³Physics and Astronomy
University of Manitoba
Winnipeg, Manitoba, Canada
Tel: +1 (204) 474-9817

Abstract

We present a repository of multi-static, near-field microwave scattering measurements. The data are presented both raw (uncalibrated), and calibrated with a scattered-field calibration. Measurements were taken with 24 co-resident Vivaldi antennas in a single plane, inside an air-filled microwave tomography system. The antennas were linearly polarized in the vertical direction, and we intended for the two-dimensional transverse magnetic (scalar) approximation to apply. Data are presented for seven targets, both metallic and dielectric, with varying geometrical complexity. Data from simple geometric targets, useful for calibration using analytic equations, are given. The repository is available from the Web site: <http://www.ece.umanitoba.ca/lovetri/EMILab/index.html>.

Keywords: Microwave imaging; inverse problems; nondestructive testing; microwave measurements; radar Imaging; measurement techniques; calibration; electromagnetic scattering; microwave tomography

1. Introduction

A common issue in the inverse-scattering community is a lack of experimental scattering data. Experimental data is required to prove that imaging algorithms, which are typically first tested on synthetic data, will provide useful images in the real world. Databases such as the Ipswich (e.g., [1-4]) and Fresnel (e.g., [5-7]) databases have partially addressed this insufficiency. The Ipswich and Fresnel data were collected with a bistatic, mechanically scanned system, with antennas located in the far field. However, there are many applications, such as biomedical imaging or nondestructive testing, for which scattering data are better collected with a mechanically static near-field system. Advantages of near-field imaging include higher resolution [8,9], but additional complications such as antenna coupling and a complicated incident field do occur. We are aware of one repository of near-field multi-static data [10], but this dataset is available pre-calibrated, with closely coupled antennas removed, and at a single frequency.

With the goal of stimulating research for both imaging/inversion and calibration, we present a database of microwave scattering measurements for a near-field multi-static microwave tomography system. Measurements are presented both calibrated and uncalibrated. The measurements were taken with the imaging system outlined in a previous publication [11]. Targets were elongated in the z direction, and the linearly polarized antennas were oriented in the same direction: we thus intended for the two-dimensional transverse magnetic (scalar) approximation to apply. Several dielectric and metallic targets were interrogated in an air background. The data are multi-static (i.e., $S_{x,y}$), and for most targets, are in the frequency range of 3 GHz to 6 GHz in 0.5 GHz steps.

Inversion results for these targets were presented in several different sources [8, 11-15]. The repository is available from the Web site:

<http://www.ece.umanitoba.ca/lovetri/EMILab/index.html>.

When the repository is used, please cite this paper. If readers have any further questions and or requests, we encourage them to contact the authors.

2. System Description

The microwave imaging system used to collect the data was described in [11]. A photograph of the system is shown in Figure 1, an antenna close-up is shown in Figure 2, and a schematic of the chamber is shown in Figure 3. The system consisted of 24 double-layer Vivaldi antennas, supported inside a Plexiglas imaging chamber. The antennas had an operating bandwidth from 3 GHz to 10 GHz (as defined by an $S_{1,1}$ below -10 dB). The antennas were described in detail in [16, 17].

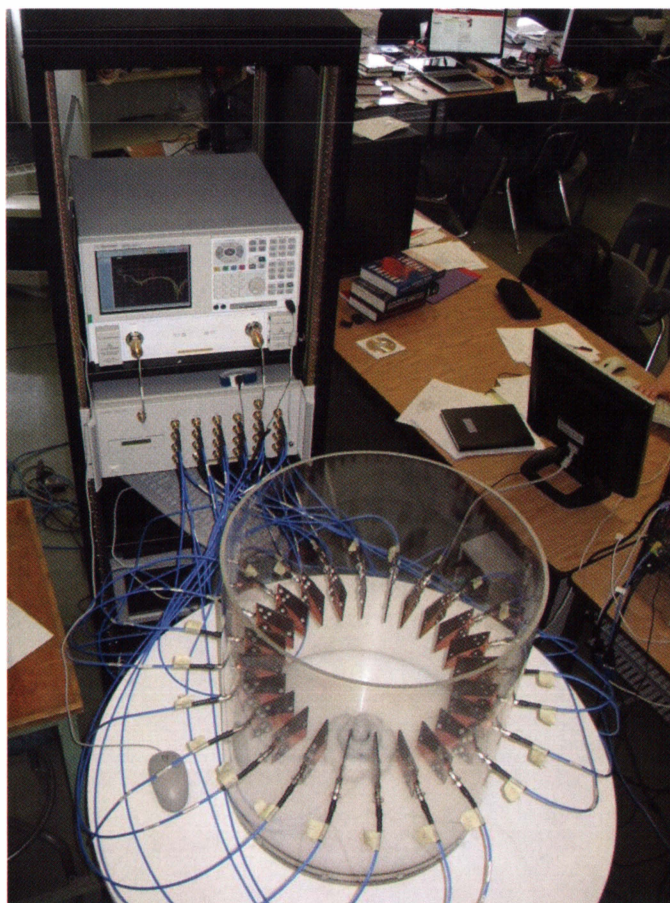


Figure 1. The wideband microwave tomography system. The 24 Vivaldi antennas were connected to a network analyzer via a 2×24 switch.



Figure 2. A close-up of one of the double-layered Vivaldi antennas used in the microwave imaging system. The two layers were held together with nylon screws.

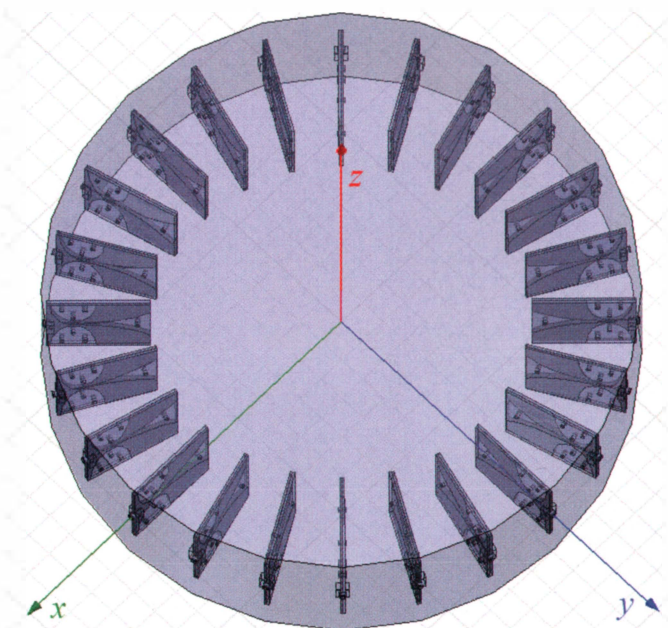
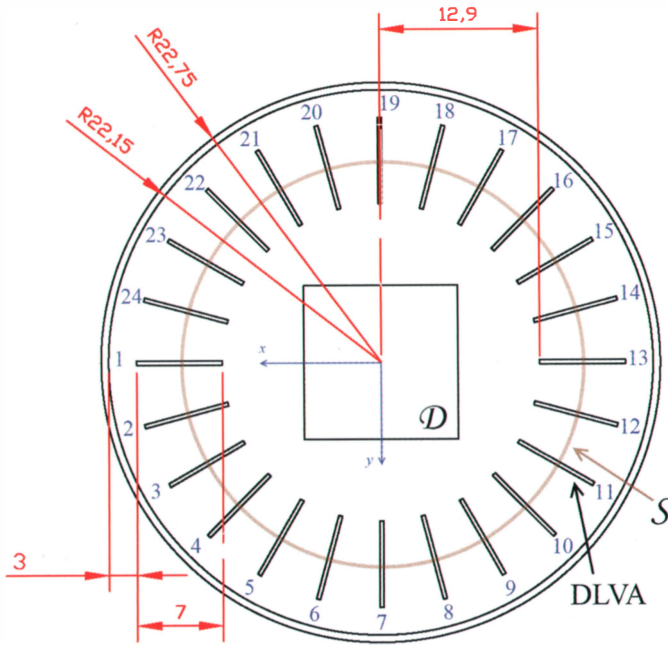


Figure 3. Schematics of the imaging system.

Additional behavior of the antennas when co-resident in the chamber was available in [11]. We note that the antennas were slightly modified from the version presented in [11, 16, 17]: the antennas were coated with a waterproof coating, which only slightly changed the characteristics of the antennas.

The microwave transmitter/receiver consisted of a two-port Agilent 8363B PNA-Series vector network analyzer (VNA). The vector network analyzer was connected to the antennas with a 2×24 crossbar mechanical switch (Agilent 87050A-K24), which provided port isolation of greater than 95 dB over the frequency range of interest.

The exterior Plexiglas cylinder had an inner radius of 22.4 cm. Each Vivaldi antenna was 7 cm long, and the base was held 3.0 cm from the wall by the connectors. The tip of the antenna was thus located 10 cm from the edge of the wall. The maximum imaging domain, D , consisted of a circle of radius 12.4 cm, located at the center of the chamber. If a square domain is used, the maximum size is a length of ≈ 18 cm. In practice, we have used a maximum imaging domain, D , with 14 cm sides, and all targets fit inside the 14 cm \times 14 cm imaging domain (and most fit into a smaller domain).

During data collection, the chamber was surrounded by radar-absorbing material (RAM): see Figure 6 for an example.

3. Data Description

For the main data set, we made measurements for six targets, plus two empty-chamber (incident-field) measurements. The target names and associated file names are listed in Tables 1 and 2. For Tables 1 and 2, the incident-field meas-

Table 1. Tomographic dataset #1: a list of the uncalibrated data files.

Description	File Name
Incident 1	tomographic_incident.txt
Incident 2	tomographic_incident_2.txt
Metal cyl. #1	tomographic_metal_2p0_inch_diam.txt
Metal cyl. #2	tomographic_metal_3p5_inch_diam.txt
Nylon cyl. #1	tomographic_nylon_4p0_inch_diam.txt
Nylon cyl. #2	tomographic_nylon_1p5_inch_diam.txt
Two nylon cyl.	tomographic_nylon_cyls_0p5cm.txt
e-phantom	tomographic_e_phantom.txt

Table 2. Tomographic dataset #2 lossy target: list of data files.

Target Name	File Name
Incident	incident_3.txt
Metal cyl. (3.5 inch)	metal_3p5_inch_diam.txt
wood and nylon	wood_and_nylon_diel.txt

Table 3. Tomographic datasets: list of calibrated data files (scattered field).

Target Name	File Name for u^{sct}
Metal cyl. #1	tomographic_metal_2p0_inch_calibrated.txt
Nylon cyl. #1	tomographic_nylon_4p0_inch_calibrated.txt
Nylon cyl. #2	tomographic_nylon_1p5_inch_calibrated.txt
Two nylon cyl.	tomographic_nylon_cyls_0p5cm_calibrated.txt
e-phantom	tomographic_e_phantom_calibrated.txt
wood and nylon	wood_and_nylon_calibrated.txt

urement number one was taken at the beginning of the data-collection process, and incident-field measurement number 2 was taken as the final data set (after data from all other targets were collected). Comparing the two incident measurements can provide an estimate of the repeatability/ noise associated with the measurements (including temporal drift, any possible changes in the scattering environment, etc.). For the bulk of the data set, measurements were taken from 3 GHz to 6 GHz in 0.5 GHz steps. All data sets had 24×23 transmission measurements of $S_{a,b}$ (reflection measurements, $S_{a,a}$, were excluded from these data).

All uncalibrated data (Tables 1 and 2) were “total field” measurements. To obtain scattered-field S parameters for a particular target, one of the incident-field measurements must thus be subtracted.

Calibrated-data file names are presented in Table 3. These data were the calibrated *scattered* fields from the measurements in Tables 1 and 2. Data were calibrated with the process outlined in Section 4.

During data collection, the vector network analyzer was calibrated to its own ports. The effects from the cables between the vector network analyzer and the switch, the internal paths of the switching matrix, and the cables from the switch to the antennas (plus associated connectors) are thus in the measurement. These effects are readily removed via a scattered-field calibration (see Section 4).

3.1 Lossy Target Data Set

For a lossy target, we also included another measurement of a wood-nylon phantom, plus associated incident and metallic cylinder files. Data were collected for frequencies of 3 GHz to 10 GHz in 1 GHz steps. Again, uncalibrated data were total-field measurements, and calibrated data were the scattered field. The files are described in Table 2. These data were collected on a different day with an older version of the data-collection software, and are thus presented separately. Calculation of scattered parameters as well as calibration should stay within the particular data set (as described in Tables 1 and 2).

3.2 A Note on the Reciprocity of Raw Data

In general, the raw data for the tomographic measurements were not reciprocal. That is, $S_{a,b} \neq S_{b,a}$. For ease of implementation, we utilized a single transmitter from the vector network analyzer, and when this was done, the internal paths in the switch were not the same length for the two scenarios. For example, when transmitting from port “a” and receiving on port “b,” the total path length in the switch was different from receiving on port “a” and transmitting on port “b.” This difference primarily affected the phase of the raw measurement, and can be removed via calibration.

3.3 File Description

For dataset #1, listed in Table 1, the general format is in seven columns. In order, these describe the frequency of operation (in GHz), the transmitter number (1-24), the receiver number (1-24), two columns of zeros, the real part of $S_{a,b}$, and the imaginary part of $S_{a,b}$. The two columns of zeros may be ignored: these columns were intended to record the elevation and angle of a positioning motor [18], which was not used for these data.

For dataset #2, listed in Table 2, the general format is in five columns. The order is the same as the previous tomographic dataset, but with the two columns of zeros removed.

For the calibrated data the file format is the same, but now the last two columns represent the real and imaginary part of the calibrated scattered field, u^{sct} .

4. Data Calibration

All data were presented in a raw, uncalibrated format. While one of the goals of this database is to encourage calibration research, we have also provided the calibrated data for each target. The calibration process is outlined below, and the calibration target was the 3.5 in diameter metallic cylinder (shown in Figure 4).



Figure 4. Metallic cylinders.

There are two main purposes of calibration: (1) to convert the $S_{a,b}$ values measured by the vector network analyzer into field values ($u = E_z$) used in the inversion algorithms, and (2) to eliminate/compensate for modeling error and other errors. We define modeling error as any mismatch between the assumed computational model and the physical measurement system (e.g., a two-dimensional scalar Green's function versus the true three-dimensional vector wave propagation).

To perform the calibration, we first measured scattered data from a known cylinder placed in the center of the chamber. Typically, we used one of the metallic cylinders, but one could also use the nylon cylinders, as well. We denoted these S parameters as $S_{a,b}^{sct,known}$. Next, we considered the S parameters from the object we wished to image (e.g., the e-phantom), and we denoted these S parameters as $S_{a,b}^{sct,unknown}$. Assuming a two-dimensional line-source-generated incident field, located at 2 cm from the tip of the antenna, we calculated the analytical scattered fields (under the two-dimensional TM assumption) from the known object, and labeled them u_{known}^{sct} . The incident field is thus the Green's function of the two-dimensional problem, with the transmitter located at a radius of 14.4 cm. These values may be calculated analytically for metallic or dielectric cylinders [19].

Finally, the calibrated measured fields for the unknown target were calculated by

$$u_{cal}^{sct} = \frac{u_{known}^{sct}}{S_{a,b}^{sct,known}} S_{a,b}^{sct,unknown}. \quad (1)$$

The process was repeated independently for every transmitting/receiving pair. This method of calibration eliminated any errors that were constant over the two measurements ($S_{a,b}^{sct}$ known and unknown). Examples of these types of “removable” errors included cable losses and phase shifts, or mismatches at connectors. However, there were other factors in the measurements that were not constant between the two measurements, and thus not entirely removed via the above calibration method. For example, the antenna factor was not guaranteed to be the same for the known and unknown measurements (as the system was operating in the near field). Another error that was not entirely compensated for was the antenna coupling, as the coupling changed when different scatterers were present in the chamber. For these reasons, we expect that the known object should be as similar as possible to the expected class of unknown target.

5. Target Descriptions

5.1 Metallic Targets

Data were collected for two metallic cylinders. The cylinders are shown in Figure 4. Metallic cylinder #1 was a hollow steel cylinder, with an outer diameter of 2 in ($d = 5.08$ cm) and a length of 65 cm. Metallic cylinder #2 was an aluminum cylinder, with an outer diameter of 3.5 in ($d = 8.89$ cm), and a length of 46 cm. For both metallic cylinder datasets, the cylinders were centered in the chamber, and no other targets were present.

5.2 Nylon Targets

There were three different nylon targets used in the University of Manitoba data. Nylon-66 was used, and the permittivity values were given in the appendix of [19]. At 3 GHz, the permittivity was expected to be $\epsilon_r = 3.03 - j0.03$. Three different cylinders were used: a large cylinder, with a diameter of 4 in ($d = 10.16$ cm) and a length of 50 cm, and two smaller cylinders, with diameters of 1.5 inches ($d = 3.81$ cm) and lengths of 44 cm. The cylinders are shown in Figure 5a.

Three sets of scattering parameters were collected with these cylinders. “Nylon #1” consisted of the large 4 in diameter cylinder centered in the chamber. “Nylon #2” consisted of a single 1.5 in diameter cylinder in the center of the chamber. The third experiment, “Two Nylon Cyl.,” consisted of two 1.5 in diameter cylinders, placed 0.5 cm apart. A photograph of these cylinders in the imaging chamber is shown in Figure 5.



Figure 5a. A photograph of the nylon-66 cylinders.

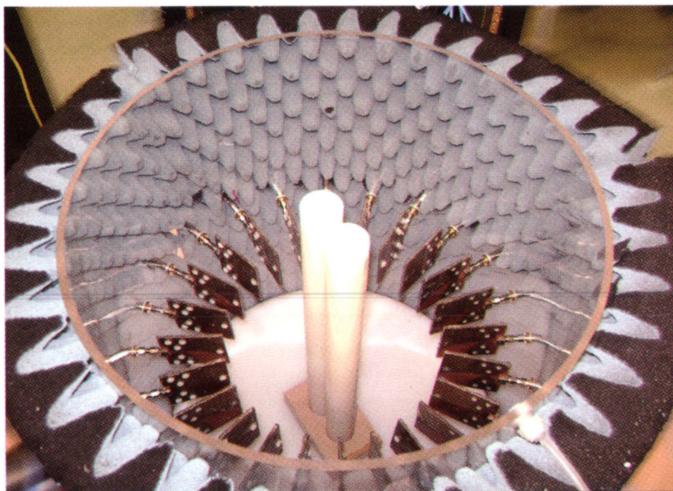


Figure 5b. The smaller two nylon-66 cylinders in the imaging chamber, 0.5 cm apart.

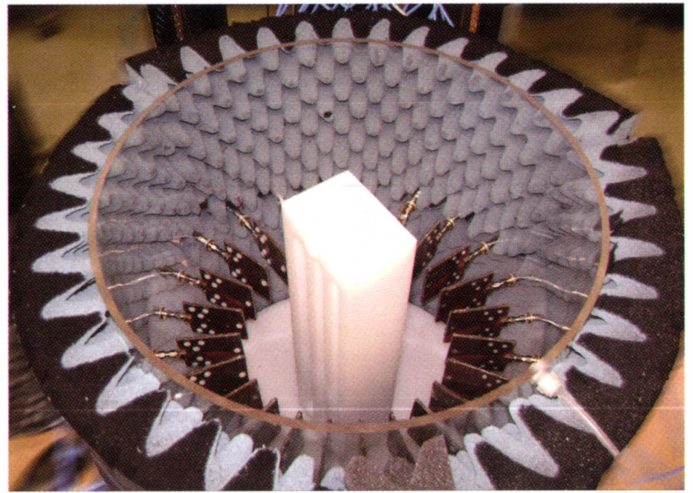


Figure 6a. A photograph of the e-phantom in the imaging chamber.

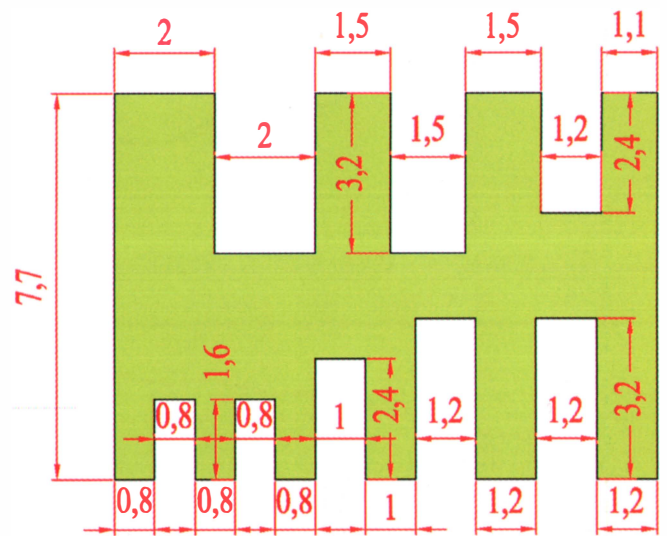


Figure 6b. A detailed schematic showing the full dimensions of the e-phantom in cm.

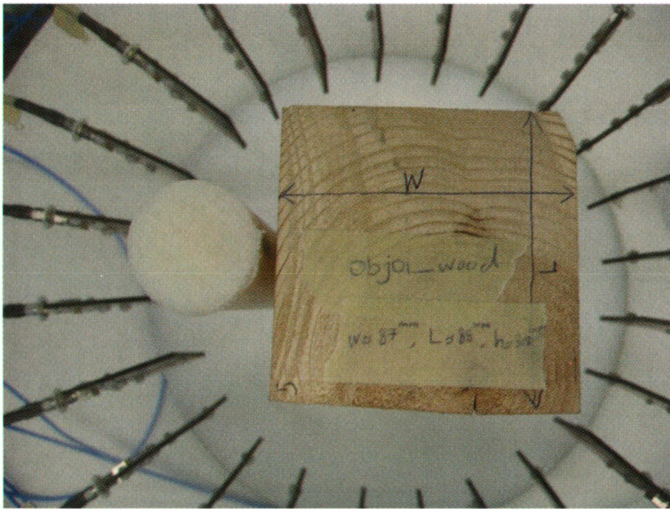


Figure 7a. A photograph of the wood and nylon phantom.

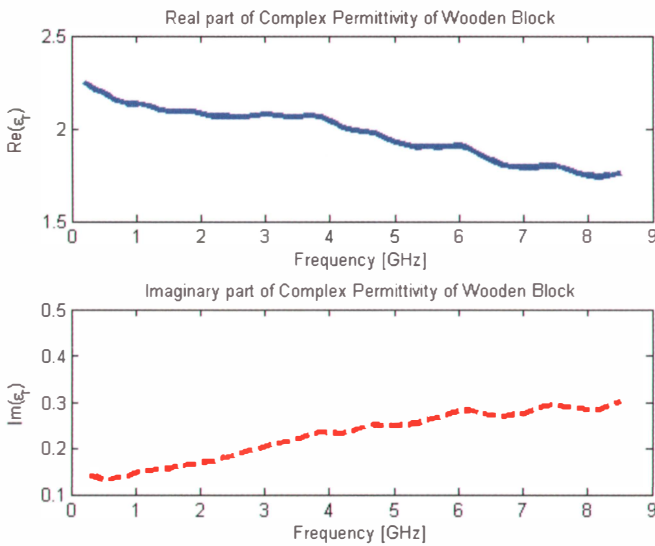


Figure 7b. A plot of the measured real and imaginary part of the permittivity of the wood block.

5.3 E-Phantom

Geometrically, the most complicated target was the e-phantom. A photograph and schematic are shown in Figure 6. The phantom was constructed from ultra-high-molecular-weight polyethylene, which had an expected permittivity of $\epsilon_r = 2.3$ at 5 GHz, with negligible loss [20].

5.4 Wood and Nylon Phantom

The wood and nylon phantom is shown in Figure 7. The phantom consisted of a 1.5 in diameter nylon-66 cylinder next to a wood block of dimensions 8.7 cm \times 8.8 cm and a height of 31 cm (the block was an untreated spruce “4 \times 4” wood construction post). The permittivity of the wood was measured

via an Agilent 85070 open-ended coaxial probe kit from 0.2 GHz to 8.5 GHz, and the values are presented in Figure 7.

6. Conclusion

It is our hope that other researchers use these data to improve inversion and calibration techniques. As further data are collected by the University of Manitoba Electromagnetic Imaging Group, we plan on posting those data, as well.

7. References

1. R. W. McGahan and R. E. Kleinman, “Special Session on Image Reconstruction using real data,” *IEEE Antennas and Propagation Magazine*, **38**, 3, June 1996, pp. 39.
2. R. V. McGahan and R. E. Kleinman, “Second Annual Special Session on Image Reconstruction Using Real Data,” *IEEE Antennas and Propagation Magazine*, **39**, 2, April 1997, pp. 7-9.
3. R. V. McGahan and R. E. Kleinman, “Third Annual Special Session on Image Reconstruction Using Real Data, Part 1,” *IEEE Antennas and Propagation Magazine*, **41**, 2, April 1999, pp. 34-36.
4. G. F. Crosta, “The Third Annual Special Session on Image Reconstruction Using Real Data. 2. The Application of Back-Propagation Algorithms to the Ipswich Data: Preliminary Results,” *IEEE Antennas and Propagation Magazine*, **41**, 2, April 1999, pp. 20-26.
5. K. Belkebir and M. Saillard, “Special Section: Testing Inversion Algorithms Against Experimental Data,” *Inverse Problems*, **17**, 2001, pp. 1565-1571.
6. J-M Geffrin, P. Sabouroux, and C. Eyraud, “Free Space Experimental Scattering Database Continuation: Experimental Set-Up and Measurement Precision,” *Inverse Problems*, **21**, 2005, pp. S117-S130.
7. A. Litman and L. Crocco, “Testing Inversion Algorithms Against Experimental Data: 3D Targets,” *Inverse Problems*, **25**, 020201, 2009.
8. C. Gilmore, P. Mojabi, A. Zakaria, S. Pistorius, and J. LoVetri, “On Super-Resolution with an Experimental Microwave Tomography System,” *IEEE Antennas and Wireless Propagation Letters*, **9**, 2010, pp. 393-396.
9. T. J. Cui, W. C. Chew, X. X. Yin, and W. Hong, “Study of Resolution and Super Resolution in Electromagnetic Imaging for Half-Space Problems,” *IEEE Transactions on Antennas and Propagation*, **52**, June, 2004, pp. 1398-1411.

10. J. J. Mallorqui, N. Joachimowicz, J. Ch. Bolomey, and A. P. Broquetas, "Database of 'In-Vivo' Measurements for Quantitative Microwave Imaging and Reconstruction Algorithms Available," *IEEE Antennas and Propagation Magazine*, **37**, 1995, pp. 87-89.
11. C. Gilmore, P. Mojabi, A. Zakaria, M. Ostadrahimi, C. Kaye, S. Noghianian, L. Shafai, S. Pistorius, and J. LoVetri, "A Wideband Microwave Tomography System with a Novel Frequency Selection Procedure," *IEEE Transactions on Biomedical Engineering*, **57**, April, 2010, pp. 894-904.
12. C. Gilmore, P. Mojabi, and J. LoVetri, "Comparison of an Enhanced Distorted Born Iterative Method and the Multiplicative-Regularized Contrast Source Inversion Method," *IEEE Transactions on Antennas and Propagation*, **57**, 8, August, 2009, pp. 2341-2351.
13. P. Mojabi and J. LoVetri, "A Pre-Scaled Multiplicative Regularized Gauss-Newton Inversion," *IEEE Transactions on Antennas and Propagation*, **59**, 2011, pp. 2954-2963.
14. A. Zakaria, C. Gilmore, and J. LoVetri, "Finite-Element Contrast Source Inversion Method for Microwave Imaging," *Inverse Problems*, **26**, 115010, 2010.
15. P. Mojabi, J. LoVetri, and L. Shafai, "A Multiplicative Regularized Gauss-Newton Inversion for Shape and Location Reconstruction," *IEEE Transactions on Antennas and Propagation*, doi: 10.1109/TAP.2011.2165487, pp. 1.
16. M. Ostadrahimi, S. Noghianian, L. Shafai, A. Zakaria, C. Kaye, and J. LoVetri, "Investigating a Double Layer Vivaldi Antenna Design for Fixed Array Field Measurement," *International Journal of Ultra Wideband Communications and Systems*, **1**, 2010, pp. 282-290.
17. M. Ostadrahimi, S. Noghianian, and L. Shafai, "A Modified Double Layer Tapered Slot Antenna with Improved Cross Polarization," 13th International Symposium on Antenna Technology and Applied Electromagnetics (ANTEM), Banff, Alberta, Canada, February 15-18, 2009.
18. C. Kaye, C. Gilmore, P. Mojabi, D. Firsov, and J. LoVetri, "Development of a Resonant Chamber Microwave Tomography system," *Ultra-Wideband, Short Pulse Electromagnetics 9*, New York, Springer, 2010, pp. 481-488.
19. R. Harrington, *Time-Harmonic Electromagnetic Fields*, New York, IEEE Press, 2001.
20. W. S. Bigelow and E. G. Farr, "Impulse Propagation Measurements of the Dielectric Properties of Several Polymer Resins," *Measurement Notes*, **55**, 1999, pp. 1-52.

Solicitation for Measurements Corner

We welcome contributions for future installments of the Measurements Corner. Please send them to Brian Fischer and Ivan LaHaie, and they will be considered for publication as quickly as possible. Contributions can range from short notes to full-length papers on all topics related to RF measurement technology and its applications, including antennas, propagation, materials, scattering, and radar cross section. New or unique measurement techniques are of particular interest. 